School of Physics and Astronomy

MSci Dissertation

March, 2023

Quantum Information Studies in an Associated Top Quark Pair Production

Supervisor:
Dr. Federica Fabbri

ID:
2340413P

Backup Supervisor:
Dr. Mark Owen

Abstract

The entanglement between fundamental particles has never been observed at the TeV energy reached by the hadron colliders. The top and anti-top pair are one of the most promising final states for this measurement. The top quarks are ideal for quantum information studies because their spin decorrelation and hadronisation time are shorter than their lifetime. This study measured the region of phase space, where the entanglement between two top quarks can be observed using a data set generated by Monte Carlo simulations. It also investigated the effect of entanglement between the tops when an associated Z-boson was produced. The tops were reconstructed to associate the correct decay products with each top quark. The angular distribution of the leptons in their parent top rest frame was used to measure the entanglement criteria, D. The D value had to be less than $-\frac{1}{3}$ for a selected sample to be entangled. The entanglement was only observed at threshold, which rendered a narrow top pair mass range where entanglement can be observed. Therefore, widening the invariant mass window, where the entanglement could be measured, would facilitate quantum information studies. Hence, selection cuts were made using the observables to increase the invariant mass window, where the tops are entangled. The D value at 400 GeV was reduced to -0.43,-0.41,-0.46 for x_f, the number of jets, and $\cos\theta^*$, respectively. These cuts effectively removed the events in which the tops were created by the quark and anti-quark annihilation, as they are not entangled. The cuts on $\cos\theta^*$ increased the invariant mass window to 600 GeV, where entanglement could be observed.

Contents

1 Introduction

Quantum entanglement is a phenomenon of interest to many because the transmission of quantum information between entangled particles is instantaneous, despite their physical separation in space. This instantaneous transmission of information is counter-intuitive because the theory of special relativity limits how fast information can be communicated [1][2]. In quantum theory, the outcome of any system does not arise from predetermined values but is an emergent property of the system when measured [3]. The EPR paradox suggests that when measuring two systems that have interacted before, the measurement of one must not influence the other, as this would lead to a hidden variable theory [4]. However, Bell's theorem proposes that such information can be exchanged instantaneously, encouraging the study of quantum information between particles [2]. Furthermore, entanglement is the most fundamental property of a quantum system. Therefore, studying this property in fundamental particles allows us to verify if nature follows a classical or quantum theory, a very intriguing study.

Classical information stored in a computer typically utilises bits represented by 0 or 1 and has a physical interpretation of an off or on, respectively. In contrast, quantum information is stored in qubits which are the two states of a bipartite quantum system, for instance [5], the spin of a particle where 1 and 0 mean spin up or spin down, respectively [1]. In particle physics, quantum entanglement unit qubits can be modelled by a spin half particle that undergoes decay.

In an entangled pair of particles, the state of one particle, such as its spin, depends on the state of the other particle; there is a correlation between entangled particles [6]. Entanglement has been previously studied in high-energy physics using particles such as mesons, neutrinos, kaons, and photons [7]. However, it has yet to be studied in fundamental particles, such as quarks, especially at the high energies (TeV) reached by the hadron colliders. Previous studies have shown entanglement, and Bell's inequality in kaons as a qubit system characterised by their spins [8]. The spin half particles, such as a fermion, are preferred to study quantum information because their spin projections are $+\frac{1}{2}$ and $-\frac{1}{2}$. In contrast, bosons have -1,0,+1, presenting complexity in calculations related to measuring entanglement. The top quarks are fermions with a spin value of $\frac{1}{2}$, ideal for studying entanglement as they can be realised as qubits, the unit for storing quantum information [9]. Furthermore, the mass of a top quark is 173 GeV which is much higher than any other particle, including the initial state proton [10].

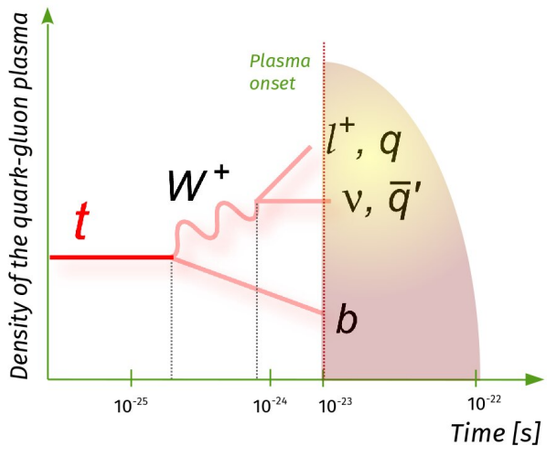

Figure 1: The figure shows the Feynman diagram of the top decay and timescale, including the lifetime of $\tau = 0.5 * 10^{-25} s$ and a spin decorrelation time of $\tau = 10^{-22} s$, and hadronisation time of $\tau = 10^{-23} s$ [11]

The top quarks have a lifetime of $\tau = 0.5 * 10^{-25} s$; they have a spin decorrelation time of $\tau = 10^{-22} s$, which is shorter than their lifetime. Thus, their spin information is effectively transferred to their decay products as it is held in their decay chain [10]. In particular, one of its decay products: lepton, has its spin entirely correlated with that of the mother top [12]. The top quarks have a hadronisation time of $\tau = 10^{-23} s$, so they decay before they can hadronise. Decaying before hadronisation would allow the study of what can be considered a bare quark [13]. Therefore, the top quarks are an excellent choice for conducting quantum information studies.

This project aims to study the entanglement between top quarks and the region of the phase space where this can be measured. A selection of cuts are applied to the top and anti-top system ($t\bar{t}$), and the effects of these cuts in terms of increasing the sensitivity to entanglement are also investigated. The cuts on the system could increase the fraction of entangled tops in the selected sample. The increased number of entangled tops facilitates the measurement of entanglement. Furthermore, the entanglement in the $t\bar{t}$ system with a production of an associated Z-boson is also analysed.

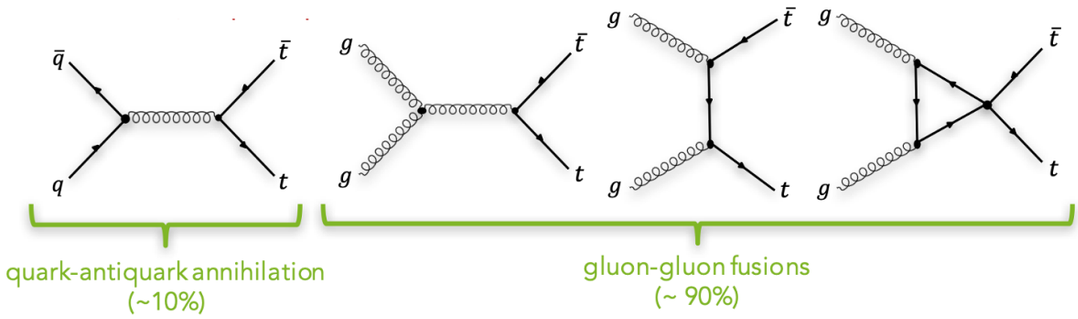

Figure 2: The figure shows the production of top quarks at LHC via gluon-gluon fusion (gg) and quark anti-quark annihilation ($q\bar{q}$) [14].

The top quarks are produced at LHC through proton-proton collision at a centre of mass (COM) energy of 13 Tev [3]; protons are composed of partons, which consist of quarks and gluons [15]. At LHC, the top quarks are produced mainly through two processes: quark and anti-quark annihilation ($q\bar{q}$) and gluon-gluon fusion (gg). The $q\bar{q}$ process accounts for 10 per cent of the production, whereas the gg process accounts for 90 per cent, as the figure 2 indicates [14]. The top quarks undergo semileptonic decay into a bottom quark and a W-boson which further decays into a pair of quarks, lepton, and a neutrino, as represented by figure 1 [13].

Afik and Muñoz (2021b) plotted the scattering angle for the gg process and $q\bar{q}$ process as a function of invariant masses. They showed that at a threshold below 400 GeV, the entangled tops are produced via the gg process [16]. This result confirms the observation by Cervera-Lierta et al. (2017), as the entanglement is only observed at low energies for top quarks, which are also spin-half fermions [17]. Furthermore, Severi et al. (2022) suggested that the transverse momentum (P_t) of the top quarks affects the entanglement due to the production process. They indicated that when the $t\bar{t}$ system has a higher transverse momentum, despite the production process of the top quarks, the system arrives at a spin-one state ($q\bar{q}$ process) due to the conservation of angular momentum [18].

Similarly, Severi et al. (2022) also studied entanglement in the $t\bar{t}$ system as a function of its scattering angle, using a helicity basis in the centre of mass (COM) frame. They found that top quarks are maximally entangled at the threshold in a spin-singlet state (spin-zero) [12]. Their spin characterises the entangled state of the top; spin-zero states result from gg fusion, and spin-one states are produced by $q\bar{q}$ annihilation [18]. The spin-triplet state is also entangled at high energies, associated with the gg process [16]. Therefore, the tops produced via the gg process are entangled, unlike those produced through the $q\bar{q}$ process [19].

The $q\bar{q}$ process can effectively be removed from the $t\bar{t}$ events by selecting a very narrow region of phase space (energy and angle of the tops) to ensure maximal entanglement of the $t\bar{t}$, as suggested by Fabbrichesi, Floreanini and Panizzo (2021) [19]. Removing events with a high P_t would also ensure this result [18]. A different approach to increasing the fraction of events created by the gg process was proposed by Aguilar-Saavedra and Casas (2022) [20]. They cut on the $t\bar{t}$ system using a parameter associated with its velocity called β. They also proposed that a cut on β (velocity) would select a spin-singlet state (spin-zero) at the threshold, causing maximal entanglement [20].

$$0 \leq C(\rho) \leq 1 \qquad [18] \tag{1}$$

The studies performed on top quarks, testing Bell's inequalities, expressed the quantum state of the tops in a density matrix ρ. The coefficients of the density matrix (ρ) were given by B_j

and C_{ij}, which are the spin polarisation matrix and the spin correlation matrix, respectively. The concurrence measures entanglement as a function of (ρ), as equation 1, illustrates. The quantum state, when maximally entangled, gives a concurrence value of one, whereas separable states, i.e. no entanglement, give a concurrence value of zero. The quantum states of the system are obtained by quantum tomography, which is performed by calculating B_j and C_{ij}. Accordingly, the conditions for entanglement are set by combining the diagonal terms of the C_{ij} matrix. The terms in the C_{ij} matrix were calculated by finding the kinematic distribution of their decay products. The kinematical distribution was given by a cross-section of the scattering process of the $t\bar{t}$ system in the rest frame of the parent particle, as expressed by equation 2 [18] [19] [16] [20] [21].

$$\frac{1}{\sigma}\frac{d\sigma}{dcos\phi_{ab}} = \frac{(1-\alpha_a\alpha_b Dcos\phi_{ab})}{2} \qquad [20] \tag{2}$$

$$\alpha_a = \alpha_b = 1 \qquad [20] \tag{3}$$

$$\frac{1}{\sigma}\frac{d\sigma}{dcos\phi} = \frac{(1-Dcos\phi)}{2} \qquad [16] \tag{4}$$

where α is the spin analysing power σ is the cross section , ϕ is the angle between the leptons in the parent top rest frame, 'a' and 'b' are the lepton from the top and the anti-top respectively.

Aguilar-Saavedra and Casas (2022), Bernreuther et al. (2004) and Afik and Muñoz (2021c) utilised the angular distribution equation as a function of α to measure the D value, as represented by the equation 2. The α is the spin analysing power, and its value equals one for leptons, as shown in the equation 3. Consequently, the angular distribution equation can be expressed in the form given by the equation 4. The 'D' in the angular distribution equation 2 and 4 provides the condition for observing entanglement. The D value is given by the trace of the spin correlation matrix C_{ij}, as represented by the equation 5 [16] [21] [20]. Therefore, the D value determines if the tops are entangled. Aguilar-Saavedra and Casas (2022) implied that the D value could be measured experimentally by fitting a line on the angular distribution plot. The D parameter measured theoretically produces a value of $\frac{-1}{3}$, which serves as the entanglement criterion, as shown in figure 3 [16].

$$D = \frac{C_{11}+C_{22}+C_{33}}{3} \qquad [20] \tag{5}$$

where C_{11}, C_{22}, C_{33} are the diagonal terms of the spin corelation matrix C_{ij}

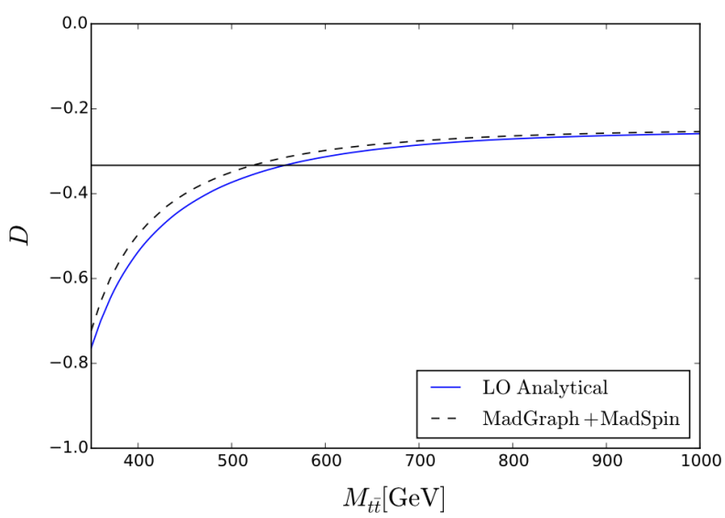

Figure 3: The plot shows the D value versus invariant mass ($M_{t\bar{t}}$), where the horizontal line provides the entanglement criterion of D = $-\frac{1}{3}$ [16].

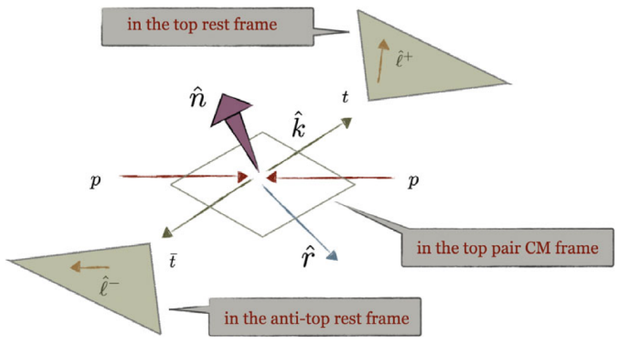

Figure 4: The figure shows the top and the anti-top coordinate system indicating the parent top rest frame and the $t\bar{t}$ rest frame [22].

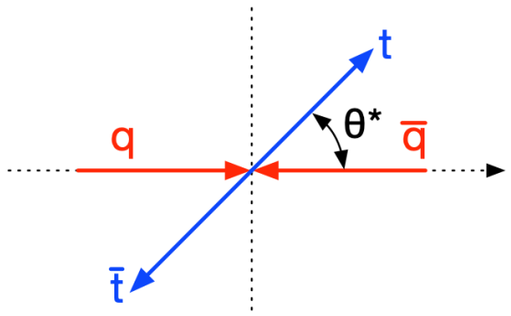

Figure 5: The figure shows the production angle of the top with respect to the initial state partons in the $t\bar{t}$ system rest frame [23].

Bernreuther et al. (2004) and Severi et al. (2022) suggested using a two-step boost to arrive at the parent top rest frame. This transformation is needed because the equation 4 only applies in the parent top's rest frame, so the reference frame of the tops has to be transformed. They first boost the z-plane in the lab frame to the $t\bar{t}$ rest frame, where the total momentum is zero. Then, boost the top directional vector defined by $\hat{k}$ to the rest frame of the tops, as represented by figure 4 [21] [12].

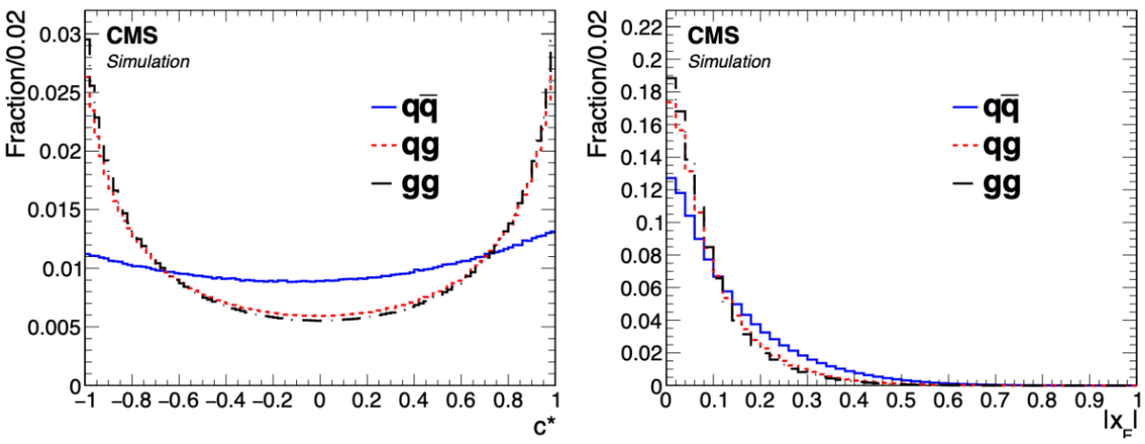

Figure 6: The plot shows observable $\cos\theta^*$ distinguishing the events created by $q\bar{q}$ and gg fusion (left).The plot shows the observable x_f distinguishing the events created by $q\bar{q}$ and gg fusion (right) [23].

In order to increase the fraction of the entangled tops, different observables can be applied as selection cuts on the $t\bar{t}$ system [12]. Sirunyan et al. (2020) used the observables $\cos\theta^*$ and x_f to measure forward-background asymmetry using events initiated only by the $q\bar{q}$ process. The $\cos\theta^*$ was defined as the production angle of the top, with respect to the initial partons, in the $t\bar{t}$ system rest frame, as shown in figure 5. The x_f is a function of the longitudinal momentum of the tops. They suggested that the gg events have a lower P_z than the $q\bar{q}$ events due to the parton distribution of the proton, in which the quarks have a higher P_t than gluons. The same paper also showed that events with a high x_f value were created by the $q\bar{q}$ process, as represented by figure 6. Based on this, this project used the observables to select only gg-initiated events [23].

2 Background Theory

2.1 The Z boson

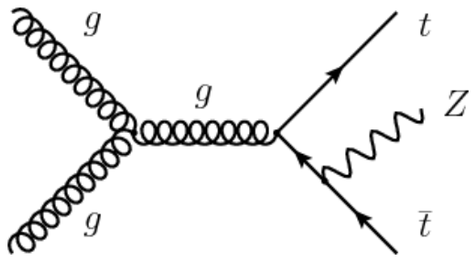

Figure 7: The figure shows the production of a Z-boson via gg fusion where it is radiated as jet by the top quark [24].

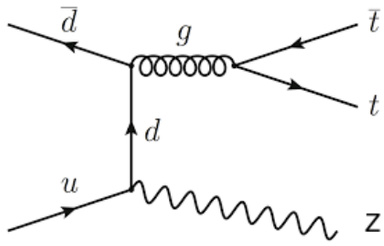

Figure 8: The figure shows the production of an associated Z-boson with the top and the anti-top via $q\bar{q}$ proccess.

The Z bosons are produced with associated top quark pairs via two processes. In the first process, it can be radiated by the top quarks created by gg fusion, as figure 7 represents. In the second process, it can be created by a $q\bar{q}$ annihilation, as shown in figure 8. The Z bosons decay into a pair of particles and anti-particles: pair of leptons, neutrinos or quarks, where the quarks further decay into jets [25]. They have a decay possibility of 10 per cent, 20 per cent, and 70 per cent, respectively [26]. For the purpose of this study, only the Z bosons decaying into light quarks are selected so the reconstruction algorithm created for the $t\bar{t}$ system could be used for this system.

2.2 Coordinate system of the ATLAS detector

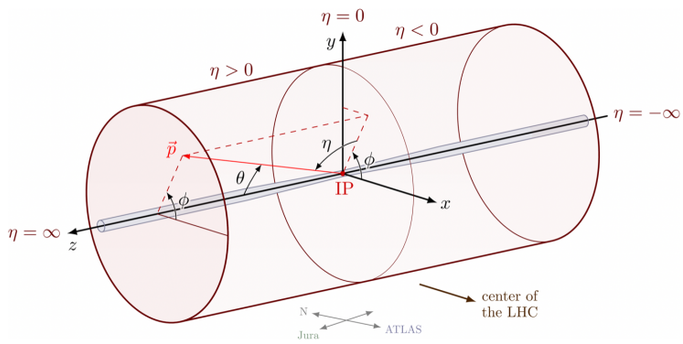

Figure 9: The figure shows the cylindrical coordinate system of the ATLAS detector representing the coordinate vectors P_t, η, and ϕ [27].

The cylindrical coordinate system of ATLAS is made of three variables: P_t, η, and ϕ, as shown in Figure 9. P_t refers to the transverse momentum of the particle after collision, perpendicular to the direction of the detector's beamline in the x-y plane. η is the pseudorapidity that describes the angle of the particle with respect to the beam axis, where its values can range from zero to positive or negative infinity in the x-z plane. ϕ is the azimuthal angle between P_t and the x-axis [28].

2.3 Kinematics and Lorentz Transformation

$$P^{\mu} = \begin{bmatrix} E \\ p_x \\ p_y \\ p_z \end{bmatrix} \quad P^{\mu}_{top} = \begin{bmatrix} E_{top} \\ \vec{p_{top}} \end{bmatrix} \qquad [29] \tag{6}$$

$$M^2_{top} = E^2_{top} - \vec{P}^2_{top} \qquad [29] \tag{7}$$

where M_{top} is the invariant mass, E_{top} is the energy, P_{top} is the momentum.

A three-dimensional vector describes three spatial coordinates, but a four-dimensional vector called a four-vector represents three spatial coordinates and a time coordinate. The energy-momentum four vectors are given by three spatial components of momentum and the energy of a particle, where energy acts as the time component in this type of four-vector. The four vectors can be transformed under Lorentz transformation, and the dot product of the four-vector with itself is invariant. The length of the four vectors remains invariant under any coordinate transformation and is called the invariant mass (M). The invariance is attributed to the rest mass, which remains constant in any inertial frame of reference. The equation 6 represents the energy-momentum four-vector of a top, and the invariant mass is represented by equation 7 [29].

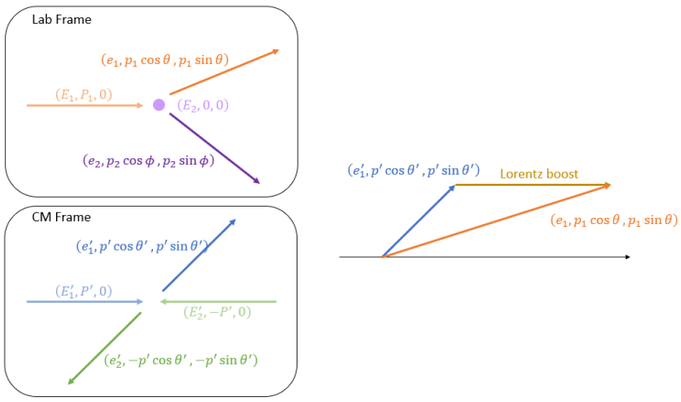

Figure 10: The figure shows the application of Lorentz boost to transform the lab frame into a COM frame, where the total momentum is zero [30].

The detector measures the particles after undergoing collision as collimated particles in the direction of the parent particle, called the lab frame [31]. Measuring the D value requires the transformation of the inertial frame of reference into the centre of mass (COM) frame where the total momentum of the top and the anti-top are zero. This transformation is possible by doing a Lorentz boost of the system where the boosted frame moves with a constant velocity with respect to the initial inertial frame, without spatially rotating the coordinates [32]. Figure 10 shows the transformation of the lab frame into the COM frame by applying Lorentz boost. Moreover, the equation 4 requires the leptons to be in the frame in which their parent top is at rest, so Lorentz boost is required.

2.4 ROOT Programme

The data processing was entirely performed through ROOT programming using the python programming language. ROOT software is a framework that enables data analysis in particle physics, which contains many helpful classes of functions that allow computation with ease. The most often performed analyses on the particle collision data, which includes calculating a four-vector, invariant mass, and Lorentz transformation can be performed using the class "TLorentzVector" within the ROOT programme [33].

3 Methods

The data for experimenting were obtained using Monte Carlo simulations (MC) and processed using the ROOT programme. At each collision event, the simulation recorded a set of decay products: leptons, Bjets, and neutrinos from the top and the anti-top. The simulated data for the Bjets and leptons contained their cylindrical coordinates P_t, η, ϕ, and E at every event. This information about the coordinates at every event was used to construct a four-vector of each decay product: Bjet, lepton, and neutrino, using the ROOT class 'TLorentzVector'.The four vectors were calculated to facilitate the measurement of the invariant mass of the system for every event.

$$t\bar{t} = l + l' + b + b' + \nu + \nu' \tag{8}$$

where l = lepton , b = bottom quark , ν = neutrino , l' = anti-lepton , b' = anti-bottom quark , ν' = anti-neutrino

The decay products were added together to produce the four vectors of the $t\bar{t}$ system, as indicated by equation 8. The four vectors of the decay products at each event were used to calculate the invariant mass of the top and the anti-top. Figure 11 indicates the invariant mass of the top. The spectrum of values for the invariant mass of the top suggests that the top was not constructed properly. The top in figure 11 had a random combination of their decay products at every event, resulting in these spectra of invariant mass values. Therefore, the top had to be reconstructed by finding the correct combination of Bjet, lepton and neutrino for every event, yielding an invariant mass value closer to its theoretical value. The algorithm that performed this computation was created using a loop that minimised the difference between the calculated invariant mass value and the theoretical value of 173 GeV. Figure 12 indicates the invariant mass of the top after the reconstruction, where nearly all events have a value closer to the theoretical value of the top, and very few events have other values, confirming a successful reconstruction of the top quark.

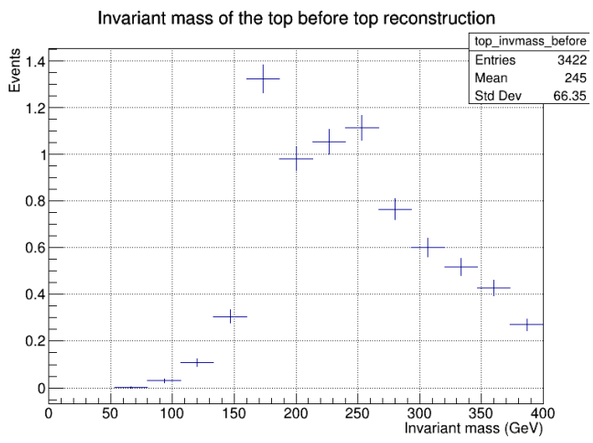

Figure 11: The plot shows the invariant mass of the $t\bar{t}$ system before reconstructing the tops where there is a spectrum of $M_{t\bar{t}}$ values.

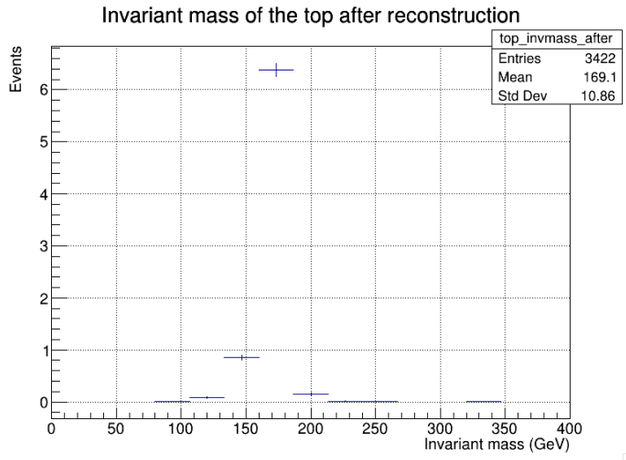

Figure 12: The plot shows the invariant mass of the $t\bar{t}$ system after reconstructing the tops where most events have $M_{t\bar{t}}$ values in agreement with the theoretical value.

The system was shifted from the lab frame to the parent top rest frame using the 'Boost' function within the TLorentzVector class. Firstly, the 'BoostVector' function was used on the top and the anti-top to obtain the three spatial dimension vectors divided by the time component. Then, the 'Boost' function was applied to the three vectors to perform a Lorentz transformation on the top and the anti-top individually, resulting in the parent top being in their rest frame.

$$cos\phi = \frac{l_+ . l_-}{|l_+||l_-|} \qquad [32] \tag{9}$$

where 'l_+' is the lepton from the top , and 'l_-' is the lepton from the anti-top

The cos ϕ of the leptons given in the equation 4 was measured by taking the dot product of the leptons using the equation 9, where l_+ and l_- are the vectors of the leptons originating from the top and the anti-top, respectively. The cos ϕ of the leptons at every event was plotted in figure 13 to enable the calculation of the D parameter, as it is a function of cos ϕ. A good strategy to measure the D value was to implement the standard equation of a line alongside the angular distribution equation (equation 4) by way of a linear fit to the cos ϕ distribution.

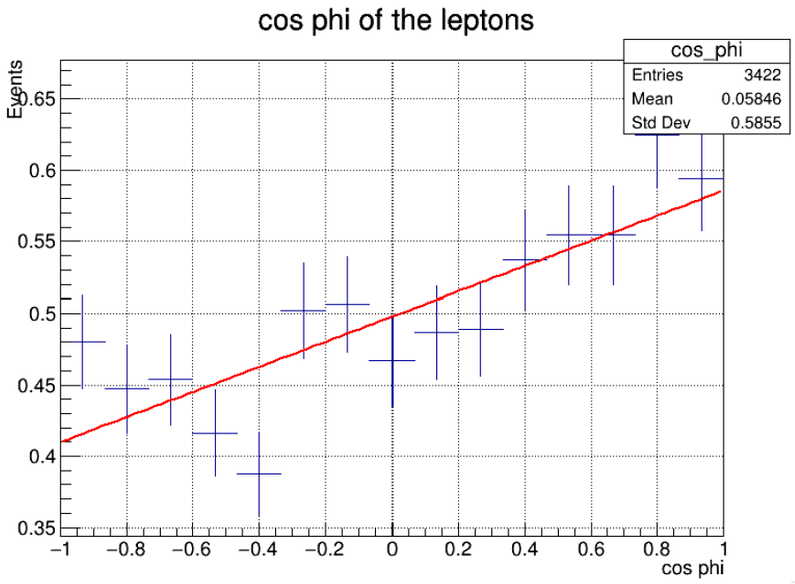

Figure 13: The plot shows the cos ϕ, the angular distribution of the leptons, for all events in the dataset. The fitted line calculates the D value for the selected sample.

$$y = mx + c \qquad [34] \tag{10}$$

where 'm' is the gradient , and 'c' is the value at y = 0

$$\frac{1}{\sigma}\frac{d\sigma}{dcos\phi} = -Dcos\phi + 0.5 \tag{11}$$

This implementation was accomplished by rearranging the angular distribution equation in the form expressed by equation 11 and comparing it to the equation of a line in the slope-intercept form as given by equation 10, where 'm' is the gradient of the line, and 'c' is the intercept. By doing so, the terms in the rearranged angular distribution equation correspond to the equation of the line, as represented by the equation 12. The D value could be extracted by calculating the value of the gradient 'm'; thus, a line was fitted on the cos ϕ plot using the rearranged equation 11.

$$y = \frac{1}{\sigma}\frac{d\sigma}{d\cos\phi}, m = -D, x = \cos\phi, \tag{12}$$

The D value was measured for events with a range of invariant masses ($M_{t\bar{t}}$) between 0 GeV to 400 Gev, 400 GeV to 450 GeV, and above 550 GeV; from these ranges, three separate graphs were made plotting their cos ϕ values for the events within those invariant mass ranges. A line was fitted in each of the cos ϕ plots using the equation 11, which provided the value of the D parameter for each case. Similarly, the D value was also calculated for all the events in the dataset, including all the $M_{t\bar{t}}$ values. Furthermore, the observables x_f and cosθ^* were computed to apply additional cuts on the $t\bar{t}$ system.

$$x_f = \frac{P_l}{\sqrt{s}} \qquad [7] \tag{13}$$

where 'P_l' is the longitudinal momentum of the system , and $\sqrt{s}$ = 13 Tev.

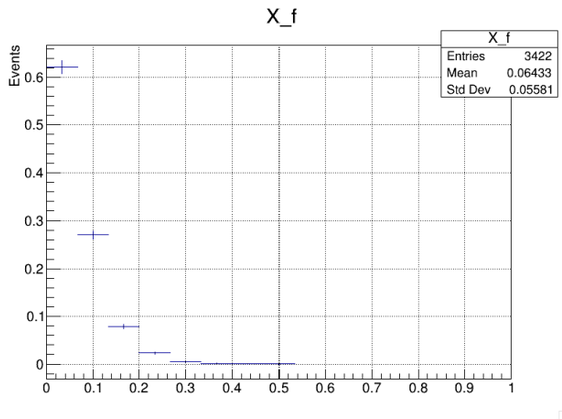

Figure 14: The plot shows the x_f values are measured for all the events in the dataset to distinguish the events produced by $q\bar{q}$ and gg process.

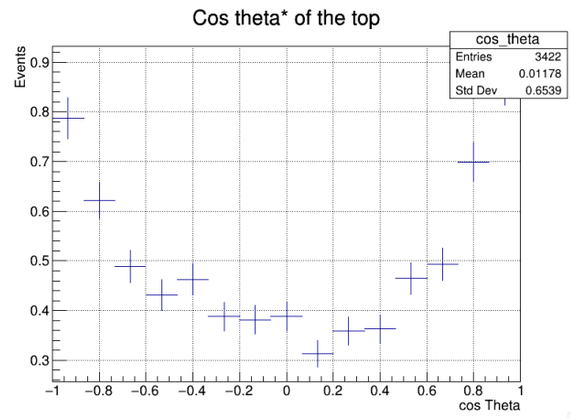

Figure 15: The plot shows the cosθ^* measured for all the events in the dataset to distinguish the events produced by $q\bar{q}$ and gg process.

The x_f parameter was calculated by taking the ratio of the longitudinal momentum of the $t\bar{t}$ system and the square root of the centre of mass energy for proton-proton collision by the equation 13. The value of x_f determines how the top and the anti-top are created. The low values of x_f correspond to the process of gluon-gluon fusion, and high x_f values to the quark anti-quark annihilation. The top and anti-top produced via gluon-gluon fusion are entangled, so the system should have low x_f values to observe entanglement between the top and the anti-top. Hence, the x_f values were calculated for all the events in the dataset and plotted in figure 14; to determine the production process of all the events obtained through MC simulations. The value of the x_f parameter for most events was less than 0.1, and relatively few events were within the range of 0.1 and 0.3. The CMS result also indicated that events with x_f values less than 0.1 correspond to gg fusion, as shown in figure 7. Therefore, the upper limit value of the x_f parameter to apply cuts on the system was set to be 0.1, as the events are more likely entangled. Additionally, the observable cosθ^* was calculated by taking the production angle of the top quark relative to the direction of the initial state parton , in the $t\bar{t}$ rest frame. The values were plotted for all events in the $t\bar{t}$ system in the range -1 to 1, as shown in figure 15.

The cuts using the x_f parameter were applied to the system to see its effect on the D value. Since only the events in which the $t\bar{t}$ system having an x_f value less than 0.1 are likely to be entangled; the three ranges of x_f values to find the range in which the D value is the lowest were selected to be between 0 to 0.03, 0.03 to 0.1, and above 0.1. For each range of x_f values, only the events in which the system has an x_f value within that range were selected. After making these selections of events according to their x_f values, the cos ϕ of their leptons in the parent top rest frame was plotted. Fitting a line on each of these cos ϕ plots provided three values of the D parameter for the three different x_f value ranges.

Jets are a collimated spray of hadrons [35] and the number of jets an event has is an observable that could be used to determine if the tops in that event are entangled. The $t\bar{t}$ event has a minimum of two jets (Bjets) but could have more, so the ideal number of jets that an event should have to observe entanglement between the tops was calculated. The D value was measured for two, three, and more than three jets. The angular distribution was plotted for all events with the selected number of jets, and a linear fit on the plot produced the D value for the respective number of jets. The calculated D values were put in a separate plot to distinguish the best selection for the number of jets to apply cuts on the $t\bar{t}$ system.

The objective was to reduce the D values, thereby increasing the $M_{t\bar{t}}$ window where the entanglement in the $t\bar{t}$ system can be observed. The D values for a range of $M_{t\bar{t}}$ values were plotted accordingly with and without additional cuts. The D value was measured for the $t\bar{t}$ system in thirteen slices of the $M_{t\bar{t}}$ spectrum. Four different selection requirements were imposed on the system where only the events meeting that required value were selected. These requirements were the observables: cosθ^*, x_f, and the number of jets. It also included the $t\bar{t}$ system without any cuts. The first slice of the $M_{t\bar{t}}$ spectrum was chosen to be between 0 Gev and 400 GeV. The consequent interval had an increment of +50 GeV, setting the second slice between 0 Gev and 450 Gev, the third slice between 0 Gev and 500 Gev, and ten more sets, including the final

slice between 0 Gev to 1000 GeV. The thirteen $M_{t\bar{t}}$ slices provided thirteen different D values for the system. This plot of D values versus the $M_{t\bar{t}}$ enabled the study of entanglement in the $t\bar{t}$ system. The study selected different observables to find the appropriate combination that would reduce the D value the most and improve the $M_{t\bar{t}}$ window where entanglement could be observed.

The $t\bar{t}$Z system was also analysed using the same techniques that were employed for the $t\bar{t}$ system. The data set was generated using MC simulations where the top and the anti-top were produced with an associated Z boson. As the study on this system followed the same methods and used the same observables, the algorithm remained the same as the one used for the $t\bar{t}$ system. Moreover, the reconstruction algorithm was kept the same because only the events in which the Z boson decays into light quarks in its final state were considered. The transverse momentum P_t of the $t\bar{t}$ system and $t\bar{t}$Z system was computed in order to understand the difference between the two systems. The D value was measured for the thirteen $M_{t\bar{t}}$ intervals of the $t\bar{t}$Z system, as done on the $t\bar{t}$ system. Likewise, the four different selection requirements used in the $t\bar{t}$ bar system were also applied to this system. These were investigated to determine if the entanglement could be observed between the top and the anti-top when an associated Z boson is produced.

4 Results and analysis

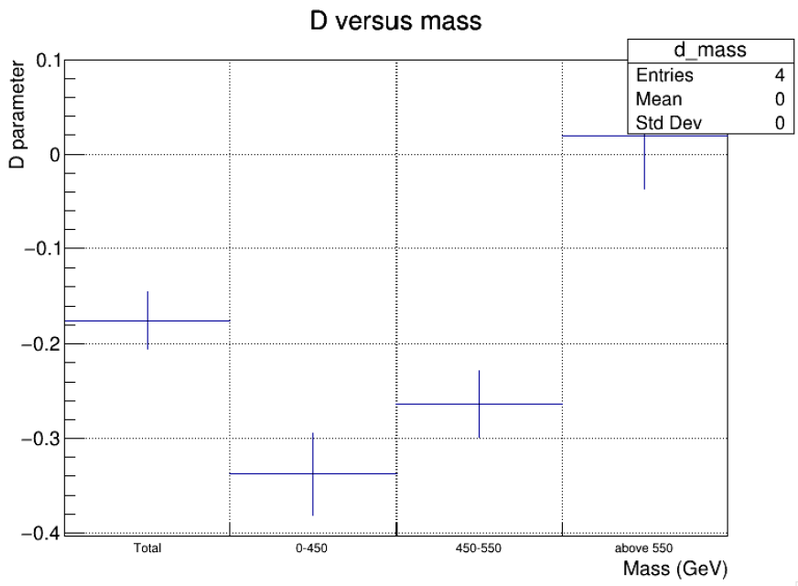

Figure 16: The plot shows the D value measured for a range of $M_{t\bar{t}}$.

The D parameter was measured for a range of $M_{t\bar{t}}$ values to find the range in which the D value was less than $\frac{-1}{3}$, indicating entanglement between the top and the anti-top. Figure 16 displays the D parameter for a range of $M_{t\bar{t}}$ of the system. The first bin in the histogram denotes the D value for the $M_{t\bar{t}}$ of the entire dataset as -0.18. The second, third, and fourth bins of the histogram represent the D value for the invariant mass window of 0 to 400 GeV, 450 to 550 GeV, and above 500 GeV, respectively. The lowest D value was measured to be -0.34 for the $M_{t\bar{t}}$ range of 0 to 450 GeV. The D value for the third and fourth bin of the histogram was -0.28 and +0.02, respectively. Therefore, a correlation between the D value and the $M_{t\bar{t}}$ suggests an increase in the D value for higher values of $M_{t\bar{t}}$.

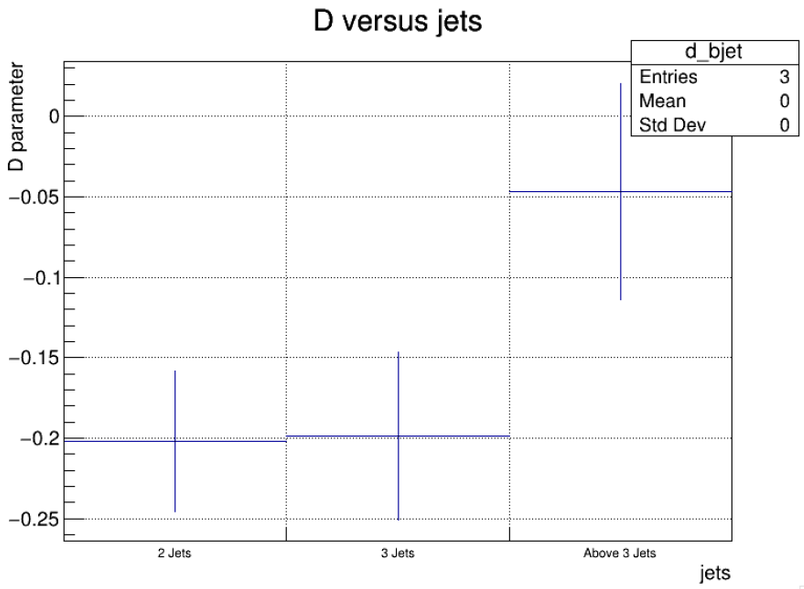

Figure 17: The plot shows the D value is measured for a range of the number of jets.

The observables used to make the selection cuts on the system to improve the $M_{t\bar{t}}$ window were: the number of jets, x_f, and cosθ^*. The cuts were applied to the top and the anti-top by selecting only the events that fall within the range of that selection criteria. Firstly, the effect that the number of jets had on the system was examined. Figure 17 denotes the number of jets versus the D parameter, where the value of D increased with an increasing number of jets. The D value for two, three, and more than three jets were calculated to be -0.18, -0.20, and -0.05, respectively. The lowest value of D was measured when the $t\bar{t}$ system had only two jets. However, when the $t\bar{t}$ system had three jets, the D value was still comparatively less than when the system had more than three jets and relatively closer to the D value at two jets.

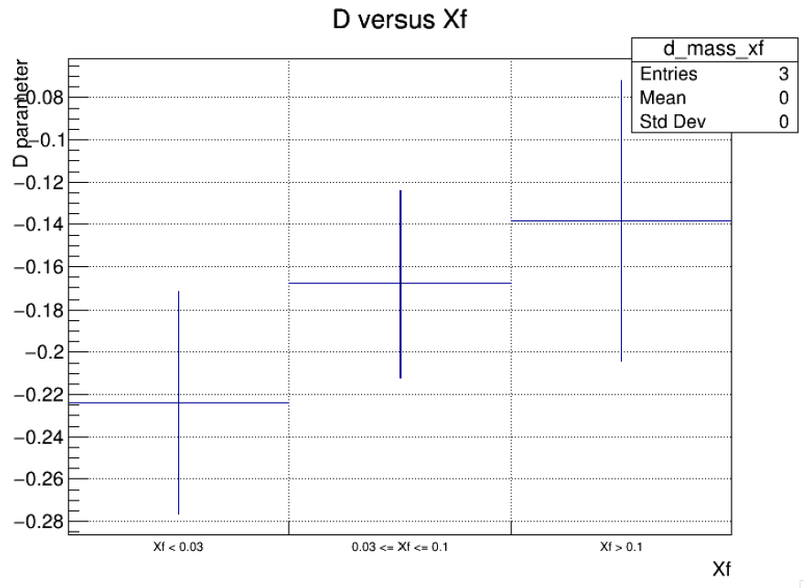

Figure 18: The plot shows the D value measured for a range of x_f values .

Secondly, the D parameter was measured for a range of x_f values as represented by figure 18; to find the range in which the value of the D parameter was the smallest. Figure 14 and 7 suggested that the x_f selection criteria be less than 0.1 as they are produced via gg fusion. Therefore, three sets of x_f range to calculate the D value were chosen to be: x_f values less than 0.03, x_f between 0.03 and 0.1, and x_f above 0.1. The D value was observed to increase for higher values of x_f, where the lowest D value was measured to be -0.22 when the value of x_f was less than 0.03. The D value was calculated to be -0.17 at x_f values between the range 0.03 to 0.1 and -0.14 at x_f values above 0.1. There was a considerable reduction in the D value when the $t\bar{t}$ system had cuts in the value of x_f compared to the number of jets. The lowest D value obtained for the system when cutting the number of jets was -0.18, whereas cutting on the x_f of the system reduced the D value to -0.22.

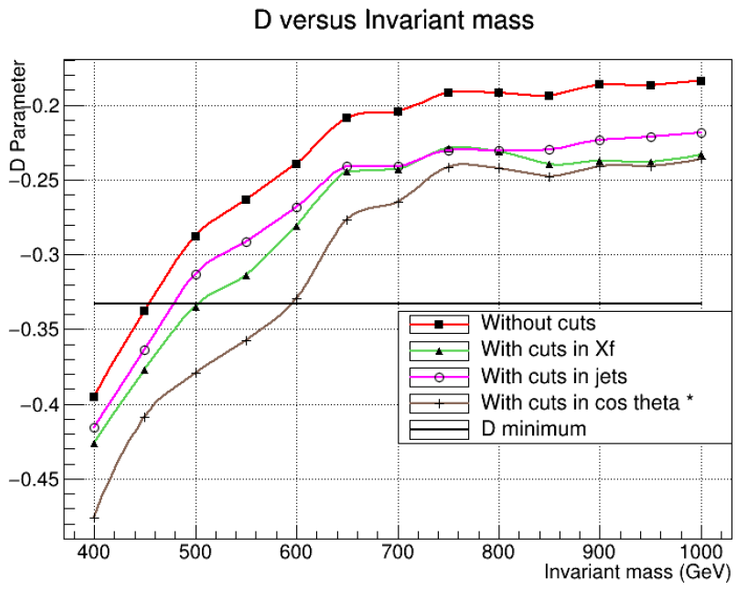

Figure 19: The plot shows the D value measured for a range of $M_{t\bar{t}}$ with and without selection cuts using the observables.

Finally, the observables x_f, the number of jets, and $\cos\theta^*$ were investigated to find the range in which the D value was the lowest, to make cuts on the $t\bar{t}$ system. Based on this analysis, the most suitable range at which the cuts on the system could be made was between 0 and 2 for the number of jets, 0 and 0.03 for the x_f values, and $cos\theta^*$ values between -0.6 to -0.1 and +0.6 to +0.1. These three selection criteria were applied to the system, and the D value was calculated for a range of $M_{t\bar{t}}$. Figure 19 indicates the D value for a range of $M_{t\bar{t}}$ where several cuts were made on the $t\bar{t}$ system using the observables.

Every point on the plot gives the D value measured for all events up to that invariant mass value. For example, at 600 GeV, the point provides the D value measured for all events with $M_{t\bar{t}}$ less than 600 GeV, i.e., between 0 GeV to 600 GeV. The straight line demonstrates the D value to observe entanglement or the criteria for entanglement at -0.33. In the $t\bar{t}$ system without additional cuts, the D value was below -0.33 for the $M_{t\bar{t}}$ range between 0 to 450 GeV. The lowest D value without any cuts on the system was measured to be -0.39 at 0 to 400 GeV. Cutting on the system using jets reduced the D value to -0.41 from -0.39 for the same $M_{t\bar{t}}$ window. Additionally, a cut on the system using x_f values reduced the D value to -0.43 and improved the $M_{t\bar{t}}$ window from 450 GeV to 500 GeV. Furthermore, the observable $\cos\theta^*$ significantly reduced the D value to -0.46, increasing the $M_{t\bar{t}}$ window to 600 GeV.

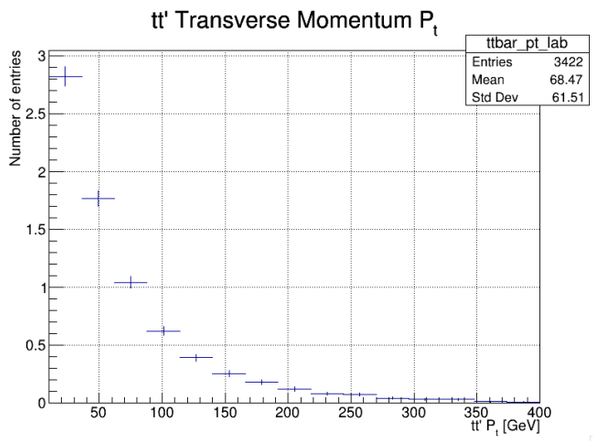

Figure 20: The plot shows the transverse momentum measured for all events in the $t\bar{t}$ system.

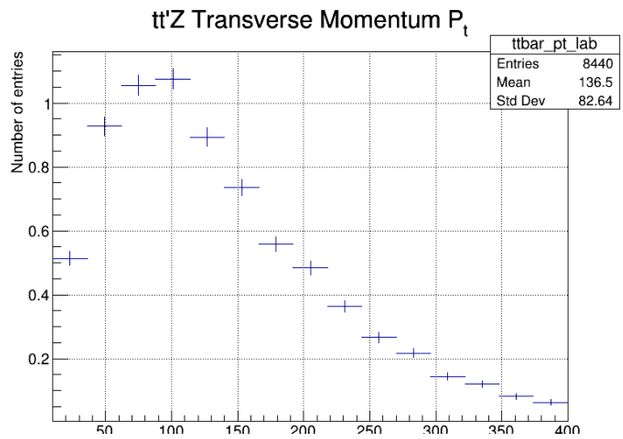

Figure 21: The plot shows transverse momentum measured for all events in the $t\bar{t}Z$ system.

The $t\bar{t}$Z process was also investigated to verify the possibility of measuring entanglement in this process. Firstly, the contrast in the kinematics of the system containing a pair of top quarks in the $t\bar{t}$ and $t\bar{t}$Z processes was studied. The variable that should be affected significantly by the presence of the Z boson ($t\bar{t}$Z) in all the events is the transverse momentum. For the conservation

of momentum, the transverse momentum (P_t) of the $t\bar{t}$ system should be zero in the absence of any additional radiation. This zero P_t is observed in figure 20, for the case of $t\bar{t}$. Figure 21 shows that the presence of a Z boson in an event drastically changes the kinematic distribution. In $t\bar{t}$Z events, the transverse momentum peak of the pair of top quarks, is indeed at 100 GeV. After verifying the capability to fully reconstruct the $t\bar{t}$ system in $t\bar{t}$Z events using the same algorithm employed in the first part of the project, the entanglement between top quarks was also tested in ttZ events.

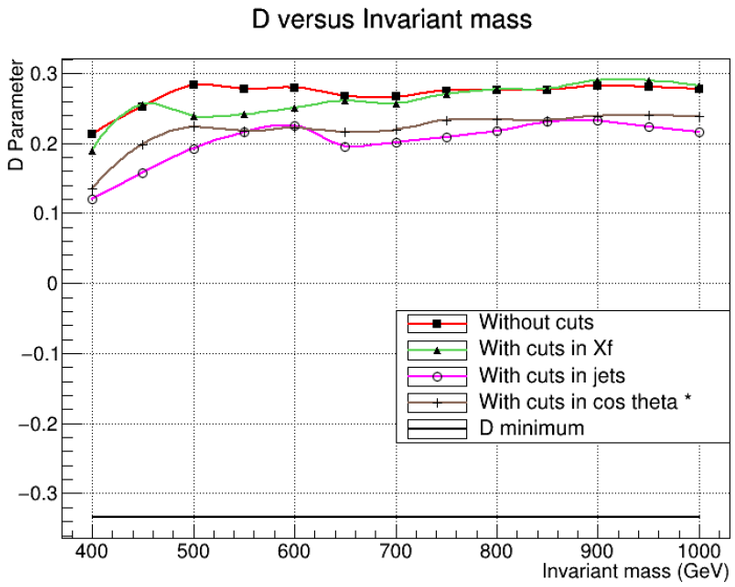

Figure 22: The plot shows the D value measured for a range of invariant mass of the $t\bar{t}Z$ system with and without selection cuts using the observables.

When an associated Z boson was produced, the D parameter was calculated for the $t\bar{t}$Z system. The D value for a range of $M_{t\bar{t}}$ was plotted in figure 22. The same observables used on the $t\bar{t}$ system was used to apply cuts, and their effects on observing entanglement within a $M_{t\bar{t}}$ range were analysed. The straight line represents the entanglement criteria at the D value equals -0.3. The system resulted in the lowest value of the D parameter for the $M_{t\bar{t}}$ range between 0 Gev to 400 GeV, which was calculated to be +0.22, when no additional cuts were applied. Cutting on the x_f value reduced the D value to +0.20 for the $M_{t\bar{t}}$ range of 0 GeV to 400 GeV. When cuts were made using cosθ^* , the D value was +0.18 for the same $M_{t\bar{t}}$ range. However, applying cuts on the system with the number of jets significantly reduced the D value to +0.12. Despite the reduction in the D value by the observables, the D value did not meet the entanglement criteria. Therefore, no entanglement was observed between the top and the anti-top in the $t\bar{t}$Z system.

5 Discussion

5.1 The measurement of D value for a range of $M_{t\bar{t}}$ values

The D parameter given by the angular distribution, equation 4, is a function of cos ϕ, the angle between the leptons in their parent top rest frame. The value of D calculated for the $t\bar{t}$ by measuring the gradient of the fitted line in the cos ϕ plot determines if the system is entangled; because when the system meets the entanglement criterion, i.e., the system has a D value of less than $\frac{-1}{3}$, the top and the anti-top are entangled. The D value was calculated for a range of $M_{t\bar{t}}$ values to study how the entanglement between the top quarks changes with the invariant mass of the system.

The D parameter measured for all the events in the entire data set returned a value of -0.18, which is considerably higher than -0.33, indicating that the events are not entangled. The lowest value of the D parameter was measured for an $M_{t\bar{t}}$ range between 0 GeV and 400 GeV. Therefore, the events where the system has a $M_{t\bar{t}}$ of less than 400 GeV are entangled. This result

is consistent with the observation by Afik and Muñoz (2021b), where the tops are entangled at a threshold below 400 GeV [16]. The D value increased proportionally to the $M_{t\bar{t}}$, particularly at values above 400 GeV. The D value between 400 and 450 GeV was -0.28 and +0.02 for $M_{t\bar{t}}$ above 550 GeV. The values of D at these $M_{t\bar{t}}$ ranges imply that $t\bar{t}$ system is not entangled when the $M_{t\bar{t}}$ of the system is above 400 GeV. The increasing D value for increasing $M_{t\bar{t}}$ values reflects the observation by Cervera-Lierta et al. (2017) where they only observed entanglement between the top quarks at low energies [17].

Observing entanglement between the top and the anti-top at energies below 400 GeV is a limiting factor, as this is a very small window. For instance, the theoretical value of the top and the anti-top system is 345 GeV, and the invariant mass upper limit where entanglement can be observed is only an additional +55 Gev from the system's threshold mass. As a result, the top and the anti-top should be reconstructed very accurately with a very low margin for error. Nevertheless, the reconstruction of the top and the anti-top is rather complex. The complexity arises due to neutrinos, a decay product that cannot be measured by the detectors. The algorithm employed in this project to reconstruct the top and the anti-top was simpler than those used at ATLAS or CMS to analyse their data.

5.2 The effect of the number of jets on the sensitivity to entanglement

The effect that the observable x_f, number of jets, and cos theta* has on the D value was measured to see if the $M_{t\bar{t}}$ window could be extended to include entanglement at higher values. Firstly, the number of jets in an event significantly impacted the system D value. D values greatly increased when there were more than three jets in an event, as shown in figure 18; when two or three jets were present, the D value was similar, around -0.20. This signifies that when the $t\bar{t}$ system has less than three jets in its final state, they are more sensitive to entanglement than events with more than three jets. Based on this data, the appropriate cut that was applied to the system was by selecting all events with less than three jets.

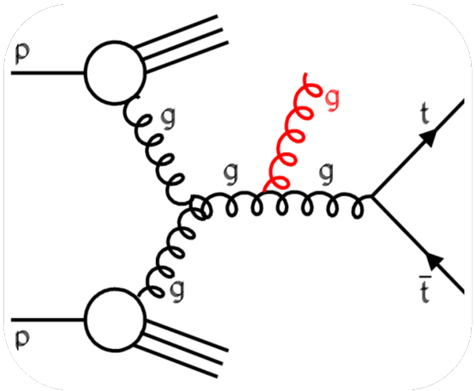

Figure 23: The figure shows the radiation of a jet by the initial state gluon which does not affect the entanglement between the tops. .

Ideally, the top quark and anti-top quark will decay into two jets, with one Bjet coming from the top and the other from the anti-top. These two jets explain the low D value of -0.18 for two jets. However, the jets could be radiated by the top quark itself or by the gluon partaking in the gluon-gluon collision. These jets radiated by either the quark or the gluon would account for the additional number of jets observed in an event. The D values for two and three jets in the system are very similar because the first additional jet, leading to three jets in a system, is most likely arising from the incoming gluon.

The figure 23 represents the incoming gluon, i.e., the gluon belonging to the gg process, radiating a jet. This jet arising from the initial state gluon does not affect the entanglement between the top quarks. Hence, there is no significant difference between the D value when the system has two or three jets. As substantiated by the results of the D value versus the number of jets, the top and the anti-top are not entangled if the top quark radiates a jet. Accordingly, an event should only contain two or three jets in its final state to observe entanglement. The $t\bar{t}$ system

is cut to only include fewer than three jets to increase sensitivity to entanglement.

5.3 The effect of the x_f value on the sensitivity to entanglement

Secondly, the effect of x_f, a function of the longitudinal momentum of the system, on increasing the fraction of top and anti-top was studied using the D parameter. The lowest D value, relatively closer to the entanglement criterion, was only measured at x_f values less than 0.03. For x_f values above 0.03, the D values increased to -0.14. The low values of x_f correspond to events in which the top and the anti-top are created by gluon-gluon fusion, as demonstrated by the CMS results [23]. Furthermore, quarks have higher momentum than the gluons, as given by the parton distribution of protons. The higher values of x_f would suggest the creation of top and anti-top via quark and anti-quark annihilation. The entanglement between the top and the anti-top is certainly affected by their production process, where only the quarks produced by gluon-gluon fusion are entangled. Hence, the suitable value of x_f to cut on the system to improve sensitivity to entanglement was 0.03.

5.4 Application of cuts on the $t\bar{t}$ system to improve the invariant mass window

The D value was plotted for the $M_{t\bar{t}}$ range starting at 0 GeV to 400 GeV and a series of ranges from 400 GeV to 1,000 GeV in increments of +50 GeV with and without cuts. When the system was analysed without cuts, the entanglement between the top and the anti-top was only observed within the 0 GeV to 450 GeV range, as indicated by the D value of -0.34 for the respective interval. This D value is expected for this interval from the invariant mass plot, represented by figure 16. Applying cuts on the system using the observables x_f, the number of jets and $\cos\theta^*$ significantly reduced the D value, thereby increasing the sensitivity to entanglement. The suitable value of the observable to make cuts on the system was determined by the D mass versus the observables plot, as represented by Figures 17, 18, and 6. The selected values were; the number of jets less than three, x_f value less than 0.03, and $\cos\theta^*$ between -0.6 to -1 and +0.6 to +1.

The cuts on the number of jets were applied to the system by only selecting events in which the total number of jets in the $t\bar{t}$ system was less than three. Two jets would mean the jets are Bjets, and no additional jets were radiated from the gluons or the quark. The two jets cut resulted in the minimum D value in the 0 to 400 GeV range decreasing to -0.41 from -0.39 without cuts. Cutting on the value of x_f by selecting the events with values less than 0.03 reduced the D value by five per cent; this extended the $M_{t\bar{t}}$ window of observable entanglement to 500 GeV. This improvement in the window was possible by selecting events with longitudinal momentum less than 0.11 GeV, effectively removing those events with high P_t, as they are created by a quark and anti-quark annihilation.

Furthermore, cutting on $\cos\theta^*$ made the most improvement in terms of extending the $M_{t\bar{t}}$ window where entanglement is observed, due to which the $M_{t\bar{t}}$ window extended to include events with invariant masses less than 550 GeV. This extension significantly improved the invariant mass window, where only events with less than 450 GeV were initially entangled. However, after applying cuts, the range of invariant masses with observable entanglement increased by +100 GeV.

The cuts on the system using $\cos\theta^*$ value proved to be the best parameter that improved the $M_{t\bar{t}}$ window on its own. The effects produced by cutting on the system using the number of jets and x_f values were very similar. The latter extended the $M_{t\bar{t}}$ window more effectively, as it had smaller D values. The combination of all three observable applied to the system to cuts on the events was attempted. However, the result was not as successful as expected in terms of further improving the invariant mass window. Applying all the cuts at once was very similar to the effect produced by applying only cuts on the $\cos\theta^*$. Therefore, cutting on the system by using the three observables separately was preferred over applying a combination of them.

The ineffective combination of the observables could be attributed to the number of events

obtained from the MC simulation. When applying the cuts, the number of events within the data set diminishes; when applied in combination, the sample size needs to be larger to visualise and extend the window of observable entanglement. Another attempt to improve the $M_{t\bar{t}}$ window was by further limiting the cosθ^* values to the ranges of -0.8 to -1 and +0.8 to +1. These tight ranges did improve the invariant mass window to include all values up to 1000 GeV. However, these cuts were unsuitable as only a few events can be expected to have a top production angle within that small range.

5.5 Application of cuts on the $t\bar{t}$Z system to improve the invariant mass window

When an associated Z boson was produced, the entanglement between the top and the anti-top was investigated using the same techniques for the system with only the top and the anti-top. The same three observables were used to cut on the system to observe its effect on improving the $M_{t\bar{t}}$ window where the system is entangled. Plotting their D values for the $M_{t\bar{t}}$ range starting at an interval 0 GeV to 400 GeV, going up to 1000 GeV, each interval with an increment of +50 GeV, showed that no entanglement can be observed between the top and the anti-top when there is a presence of a Z boson.

Cutting on the system to decrease the D values did not cause any substantial changes despite reducing the D values slightly. For a Z boson to be produced, it must be via $q\bar{q}$ annihilation and top quarks produced through the same process are not entangled. Also, the system with a Z boson has more jets than the system with only the top and the anti-top. As illustrated by figure 22, which shows the number of jets versus the D mass plot, the D value is higher than the entanglement criteria when there are three jets or more. These two factors contribute the most to the sensitivity to entanglement of the system with a Z boson. Thus, no entanglement is observed for this system due to the associated production of the Z boson.

6 Conclusion

This project aimed to study the entanglement in the top quarks and the region of phase space where this can be measured. Cutting on the $t\bar{t}$ system increased the fraction of entangled tops in a sample. The entanglement criterion was given by D = $-\frac{1}{3}$, and the D value was measured for a selected $M_{t\bar{t}}$ range. The tops were maximally entangled only below the threshold of 400 GeV. This narrow region of phase space was extended to include events with a higher $M_{t\bar{t}}$; by cutting on the system using the observables: x_f, the number of jets, and cosθ^*. The selection cuts removed the events created by the $q\bar{q}$ process, as these are not entangled. As a result, the D value was measured for the $t\bar{t}$ events in slices +50 GeV of $M_{t\bar{t}}$ between the range 400 GeV to 1000 GeV; this was performed with and without cuts. The D value without the cuts was -0.39 at 400 GeV; the values were reduced by applying the cuts. The reduced D values were -0.43,-0.41,-0.46 for x_f, the number of jets, and cosθ^*, respectively. Reducing the D value for a $M_{t\bar{t}}$ range increased the invariant mass window where entanglement can be observed. The cuts on cosθ^* produced the most significant extension in the $M_{t\bar{t}}$ window, up to 600 GeV. Furthermore, entanglement was studied in the system $t\bar{t}Z$. The endeavour to reduce the D values in the $t\bar{t}Z$ using the observables proved inconsequential. Entanglement was not observed in the $t\bar{t}Z$, including below the threshold. The radiation of a Z boson in the $t\bar{t}$ system destroys the entanglement between the two top quarks.

References

[1] University of Waterlooo. What is a qubit? https://uwaterloo.ca/institute-for-quantum-computing/quantum-101/quantum-information-science-and-technology/what-qubit#spin. [Institute for Qauntum Computing].

[2] Marco Fabbrichesi, Roberto Floreanini, and Giancarlo Panizzo. Testing Bell Inequalities at the LHC with Top-Quark Pairs. *Physical Review Letters*, 127(16), 10 2021. doi: 10.1103/physrevlett.127.161801. URL http://link.aps.org/pdf/10.1103/PhysRevLett.127.161801.

[3] Konrad Jende. When protons collide, . URL https://atlas.physicsmasterclasses.org/en/zpath_protoncollisions.htm.

[4] Markus Cristinziani and Martijn Mulders. Top-quark physics at the Large Hadron Collider. *Journal of Physics G*, 44(6):063001, 5 2017. doi: 10.1088/1361-6471/44/6/063001. URL https://doi.org/10.1088/1361-6471/44/6/063001.

[5] Jeffrey Bub. Quantum Entanglement and Information. In Edward N. Zalta, editor, *The Stanford Encyclopedia of Philosophy*. Metaphysics Research Lab, Stanford University, Summer 2020 edition, 2020.

[6] Andreas Muller. What is quantum entanglement? A physicist explains the science of Einstein's 'spooky action at a distance', 2022. URL https://theconversation.com/what-is-quantum-entanglement-a-physicist-explains-the-science-of-einsteins-spooky-action-at-a-distance-191927.

[7] Yoav Afik and De Nova Juan Ramón Muñoz. Entanglement and quantum tomography with top quarks at the LHC. *European Physical Journal Plus*, 136(9), 9 2021. doi: 10.1140/epjp/s13360-021-01902-1. URL https://link.springer.com/content/pdf/10.1140/epjp/s13360-021-01902-1.pdf.

[8] Reinhold A. Bertlmann and Beatrix C. Hiesmayr. Kaonic Qubits. *Quantum Information Processing*, 5(5): 421–440, 10 2006. doi: 10.1007/s11128-006-0026-1.

[9] M. Beneke and et al. Efthymiopoulos. Top Quark Physics. *arXiv (Cornell University)*, 3 2000. URL https://arxiv.org/pdf/hep-ph/0003033.

[10] Nello Bruscino, ATLAS Collaboration, et al. Top quark physics with the atlas detector: recent highlights. *Physica Scripta*, 95(9):094005, 2020.

[11] Ingrid Fadelli. The first evidence of top quark production in nucleus-nucleus collisions, 1 2021. URL https://phys.org/news/2021-01-evidence-quark-production-nucleus-nucleus-collisions.html.

[12] Claudio Severi, Cristian Degli Esposti Boschi, Fabio Maltoni, and Maximiliano Sioli. Quantum tops at the lhc: from entanglement to bell inequalities. *The European Physical Journal C*, 82(4):285, 2022.

[13] M Tanabashi et al. Particle data group. *Phys. Rev. D*, 98(3):030001, 2018.

[14] Geoffrey Gilles. Top quark production at the lhc. Technical report, ATL-COM-PHYS-2018-145, 2018.

[15] Markus Cristinziani and Martijn Mulders. Top-quark physics at the large hadron collider. *Journal of Physics G: Nuclear and Particle Physics*, 44(6):063001, 2017.

[16] Yoav Afik and Juan Ramón Muñoz de Nova. Entanglement and quantum tomography with top quarks at the lhc. *The European Physical Journal Plus*, 136:1–23, 2021.

[17] Alba Cervera-Lierta, Jose Ignacio Latorre, Juan Rojo, and Luca Rottoli. Maximal entanglement in high energy physics. *SciPost Physics*, 3(5):036, 2017.

[18] Yoav Afik and Juan Ramón Muñoz de Nova. Quantum information with top quarks in QCD. *Quantum*, 6:820, September 2022. ISSN 2521-327X. doi: 10.22331/q-2022-09-29-820. URL https://doi.org/10.22331/q-2022-09-29-820.

[19] M. Fabbrichesi, R. Floreanini, and G. Panizzo. Testing bell inequalities at the lhc with top-quark pairs. *Phys. Rev. Lett.*, 127:161801, Oct 2021. doi: 10.1103/PhysRevLett.127.161801. URL https://link.aps.org/doi/10.1103/PhysRevLett.127.161801.

[20] JA Aguilar-Saavedra and JA Casas. Improved tests of entanglement and bell inequalities with lhc tops. *The European Physical Journal C*, 82(8):666, 2022.

[21] Werner Bernreuther, A Brandenburg, ZG Si, and P Uwer. Top quark pair production and decay at hadron colliders. *Nuclear Physics B*, 690(1-2):81–137, 2004.

[22] Marco Fabbrichesi, R Floreanini, and G Panizzo. Testing bell inequalities at the lhc with top-quark pairs. *Physical Review Letters*, 127(16):161801, 2021.

[23] Albert M Sirunyan, Armen Tumasyan, Wolfgang Adam, Federico Ambrogi, Thomas Bergauer, Marko Dragicevic, Janos Erö, A Escalante Del Valle, Martin Flechl, Rudolf Fruehwirth, et al. Measurement of the top quark forward-backward production asymmetry and the anomalous chromoelectric and chromomagnetic moments in pp collisions at s $\sqrt{s} = 13tev$. *Journal of High Energy Physics*, 2020(6):1–56, 2020.

[24] et all chatrchyan. Measurement of associated production of vector bosons and top quark-antiquark pairs in pp collisions at $\sqrt{s} = 7TeV$. *Physical Review Letters*, 110(17), 4 2013. doi: 10.1103/physrevlett.110.172002. URL http://link.aps.org/pdf/10.1103/PhysRevLett.110.172002.

[25] Konrad Jende. Z Boson, . URL https://atlas.physicsmasterclasses.org/en/zpath_zboson.htm.

[26] Konrad Jende. More about the Z boson, . URL https://atlas.physicsmasterclasses.org/en/zpath_lhcphysics2.htm.

[27] Izaak Neutelings. CMS coordinate system, 12 2022. URL https://tikz.net/axis3d_cms/.

[28] Devin Jones. Poster: Study of Transversal Momentum, Phi, and Eta, 2014. URL https://www.i2u2.org/elab/cms/posters/display.jsp?type=paper&name=study_of_transversal_momentum_phi_and_eta-cms-daisy-fetsko-mills_godwin_high_school-henrico-va-2014.0302.data.

[29] Four-vectors in Relativity. URL http://hyperphysics.phy-astr.gsu.edu/hbase/Relativ/vec4.html.

[30] differential cross section in different frame, 9 2021. URL https://nukephysik101.wordpress.com/2011/04/26/differential-cross-section-in-different-frame/.

[31] Sebastian Schätzel. Boosted top quarks and jet structure. *The European Physical Journal C*, 75:1–68, 2015.

[32] How to Find Angle Between Two Vectors? - Formula, Examples. URL https://www.cuemath.com/geometry/angle-between-vectors/.

[33] ROOT: TLorentzVector Class Reference. URL https://root.cern.ch/doc/master/classTLorentzVector.html.

[34] Equation of Straight Line - Forms, Formula, Examples — What is Equation of Line? URL https://www.cuemath.com/geometry/equation-of-a-straight-line/.

[35] Jets at CMS and the determination of their energy scale — CMS Experiment. URL https://cms.cern/news/jets-cms-and-determination-their-energy-scale.